

## Preparation of Carboxylated Carbon Nitride for RhB Photocatalytic Degradation

<sup>1</sup>Hao Yang, <sup>1</sup>Wenjie Cheng, <sup>1</sup>Mengdi Xu, <sup>1</sup>Guijun Yang, <sup>1</sup>Huiyuan Chen, <sup>1</sup>Caihong Xue\*

<sup>1</sup>Guocai Ma\*\* and <sup>2</sup>Heqi Li\*\*\*

<sup>1</sup>Qinghai University, Xining 810016, China.

<sup>2</sup>School of Materials Science and Engineering, Harbin Institute of Technology, Harbin 150080, China.

[xuech@126.com](mailto:xuech@126.com)\*; [409921294@qq.com](mailto:409921294@qq.com)\*\*; [1617889593@qq.com](mailto:1617889593@qq.com)\*\*\*

Received on 28<sup>th</sup> April 2022, accepted in revised form 6<sup>th</sup> February 2023

**Summary:** A simple calcination process was used to create g-C<sub>3</sub>N<sub>4</sub> (CN) from melamine, and the modified g-C<sub>3</sub>N<sub>4</sub> (MCN) was synthesized with hydrochloric acid (HCl), sulfuric acid (H<sub>2</sub>SO<sub>4</sub>), and nitric acid (HNO<sub>3</sub>). After acid modification, CN successfully introduced oxygen-containing functional groups and obtained CN-HNO<sub>3</sub> with multiple holes, which improved the photocatalytic efficiency. The bandgap of CN-HNO<sub>3</sub> (2.46 eV) is 0.24 eV lower than that of CN (2.70 eV), resulting in more electron holes and improved light absorption of the catalyst. CN-HNO<sub>3</sub> has a conduction band (CB) of -1.23 eV, while CN has a CB of -1.13 eV. CN-HNO<sub>3</sub> is simpler to convert O<sub>2</sub> to ·O<sub>2</sub><sup>-</sup> than CN, which can boost photocatalytic efficiency. The degradation of rhodamine B (RhB) was used to investigate the photocatalytic properties of CN and MCN. The results show that the photocatalytic efficiency of MCN was higher than that of pure CN, and the photocatalytic efficiency and degradation rate constant of CN-HNO<sub>3</sub> was 36.6% and 5.5 times higher than that of the CN, reaching 99.7% and 0.0341 min<sup>-1</sup>. The degradation efficiency remained more than 85% after five cycles, showing that MCN was more photocatalytically stable than CN.

**Keywords:** Acid; g-C<sub>3</sub>N<sub>4</sub>; Bandgap width; Photocatalytic; Rhodamine B

### Introduction

With the continued growth of business and the worsening of environmental degradation [1], the physical and biological methods in traditional water treatment processes cannot meet sewage treatment needs [2]. Photocatalytic technology is a novel way to handle the problem of water pollution, and it has a wide range of applications in environmental pollution management. As the core of photocatalytic technology, there are various types of photocatalysts, such as TiO<sub>2</sub>, ZnO, and CN [3-7]. Among them, CN has great application prospects in photocatalysis due to an appropriate band edge, good stability, and stability in water, acid, and alkali solutions [8-12], however, because of the narrow broadband gap (2.7 eV), CN has a low visible light usage and quantum efficiency, limiting its use [13].

Several strategies for improving the photocatalytic performance of CN have been investigated to address these issues, including different metal or nonmetal doping [14, 15]. They add defects or affect the crystallinity of photocarriers by doping transition metals (TM) such as iron, cobalt, nickel, copper, and vanadium, which can act as

electron and hole traps to extend the lifespan of photocarriers. In addition, the acid treatment of CN to produce covalent bonds of oxygen groups (e.g., -COOH and -OH) on its base surface facilitates the incorporation of hydrophilic groups to change surface properties [16]. Li et al [17]. Prepared hydrophilic porous CN using K<sub>2</sub>Cr<sub>2</sub>O<sub>7</sub>-H<sub>2</sub>SO<sub>4</sub> as a chemical oxidant, with a higher surface area (235.2 m<sup>2</sup>·g<sup>-1</sup>) than that of pure CN. In addition, the bandgap of this water-dispersed porous CN was lower than that of pure CN (0.2 eV) Weight et al [18]. The use of HNO<sub>3</sub> to oxidize CN is a cost-effective and ecologically beneficial technology. Compared with bulk CN, the surface of hydrothermal oxidized CN has higher carboxyl and hydroxyl covalent functional groups, and the zeta point shows that CN has a positive charge after acid treatment, which is the main reason for the improvement of Cr (VI) adsorption. However, due to its complex preparation method, time-consuming and uneconomical shortcomings, industrializing is not easy. As a result, more research into cost-effective and efficient strategies to increase CN's photocatalytic activity is required.

---

\*To whom all correspondence should be addressed.

The active sites were developed to assist the migration of photogenerated charges, which considerably increased the separation efficiency of photogenerated electron-hole pairs of catalysts, and the causes for the differences of various acid pairs were studied in this article. On the CN-HNO<sub>3</sub> surface, there are oxygen-containing functional groups, and CN with a pore structure is formed. MCN also has a high rate of photocatalytic destruction of organic contaminants.

## Experimental

### Experimental materials

Melamine (analytically pure), concentrated nitric acid (68%), concentrated hydrochloric acid (36%), concentrated sulfuric acid (98%), RhB (analytically pure), absolute ethanol (analytically pure), all reagents purchased from Aladdin Reagent

(Shanghai) Co., Ltd., deionized water for laboratory self-made. All drugs were not further purified.

### CN preparation

5 g melamine was dried at 60 °C for 12 h, and then put into the crucible and placed in the box furnace. In the air atmosphere, a heating rate of 1 °C min<sup>-1</sup> was used to raise the temperature from room temperature to 300 °C, and then a heating rate of 4 °C min<sup>-1</sup> was used to raise the temperature from 300 to 550 °C and keep it there for 3 h. After allowing the product to cool to room temperature, it was ground and a little amount of deionized water was added. After ultrasonic 30 min, the mixed solution was centrifuged. The separated product was washed repeatedly with anhydrous ethanol, and CN was obtained after drying at 60 °C for 24 h. Fig. 1 shows the schematic diagram of CN synthesis.

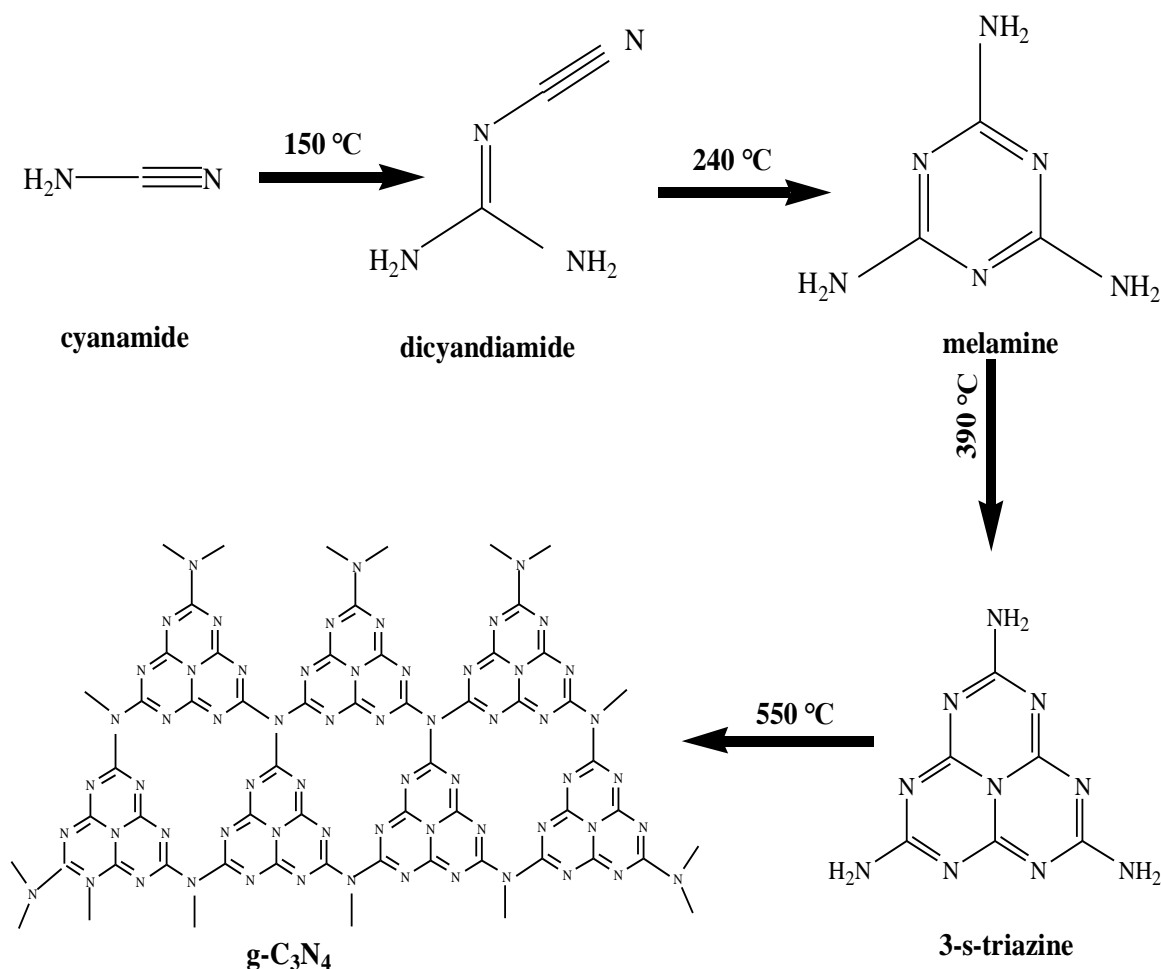


Fig. 1: Schematic diagram of CN synthesis.

### Preparation of CN modified by different acids

As shown in Fig. 2, 1 g CN solid was weighed, 30 mL concentrated acid ( $\text{HNO}_3$ ,  $\text{HCl}$ ,  $\text{H}_2\text{SO}_4$ ) was taken, and 70 mL deionized water was added. 1 g of CN was added to the solution. Reflux at  $80^\circ\text{C}$  for 12 h, then allow cooling at ambient temperature. The result of the reflux was centrifuged at 12000 rpm and rinsed with deionized water until the pH reached 7.0. Finally, the modified CN was obtained after drying at  $60^\circ\text{C}$  for 12 h in a vacuum oven. Put into the bowl grinding. The MCNs were obtained.

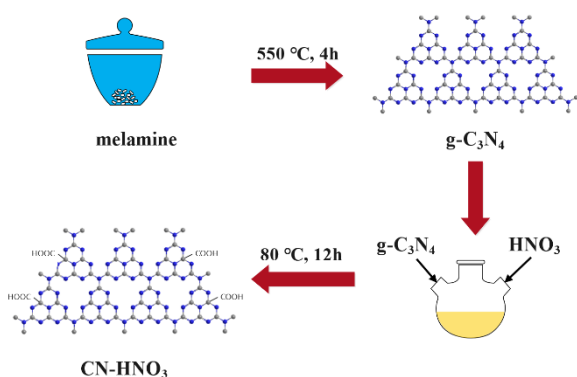


Fig. 2: Preparation diagram of  $\text{HNO}_3$  modified CN.

### Photocatalytic experiments of catalysts

Take 20 mg/L RhB solution 150 mL, weigh modifier 100 mg, and put it into RhB solution. The prepared RhB solution was placed in a xenon lamp light agitator for stirring. After a dark reaction for 30 min, the sample was centrifuged. The upper layer was taken for the UV-Vis test at night. After the test, the xenon lamp was turned on and stirred every 30 min

under the light. The samples were centrifuged. Then, the upper layer was taken for the UV-Vis test.

### Results and Discussion

Fig 3 (a) shows the XRD patterns of the CN and MCN samples with the diffraction pattern of two classic peaks, which are located at  $13^\circ$  (100) and  $27.5^\circ$  (002), corresponding to the 3-s-triazine ring in-plane structure filling and conjugated aromatic interlayer stacking. The results indicate that the XRD patterns of CN are consistent with the standard diffraction pattern of the data card JCPDS 86-2345, suggesting that the phase structure of MCN is not changed after modification. Moreover, it is noteworthy that the intensity of the sharp peaks follows the order of  $\text{CN} > \text{CN-HCl} > \text{CN-HNO}_3 > \text{CN-H}_2\text{SO}_4$ , suggesting that  $\text{CN-H}_2\text{SO}_4$  has a lower crystal structure than the other MCN the reason that the stronger the acidity is, the greater the damage is. The slight peak broadening reflects the slight deformation of the graphite structure, which may be attributed to the strength of the acid.

The functional groups of CN and MCN were characterized by FT-IR (Fig.3b). CN,  $\text{CN-HCl}$ , and  $\text{CN-H}_2\text{SO}_4$  showed no obvious special peaks. The absorption bands of MCN and CN near  $808\text{ cm}^{-1}$  correspond to the out-of-plane bending vibration mode of the heptane ring, indicating the existence of the melamine  $\text{NH}/\text{NH}_2$  group. The presence of  $\text{N}=\text{C}=\text{N}$  is attributable to the absorption band at  $900\sim 1800\text{ cm}^{-1}$ , and the peak width at  $3000\sim 3500\text{ cm}^{-1}$  corresponds to the stretching vibration absorption peak of  $-\text{NH}$  or  $\text{OH}$ .  $\text{CN-HNO}_3$  did, however, show two additional FTIR absorption peaks at roughly  $1701$  and  $1390\text{ cm}^{-1}$ , which can be attributed to the stretching modes of  $\text{C}=\text{O}$  and  $\text{NO}_3^-$ , respectively. It is proven that nitric acid modification may introduce  $-\text{COOH}$

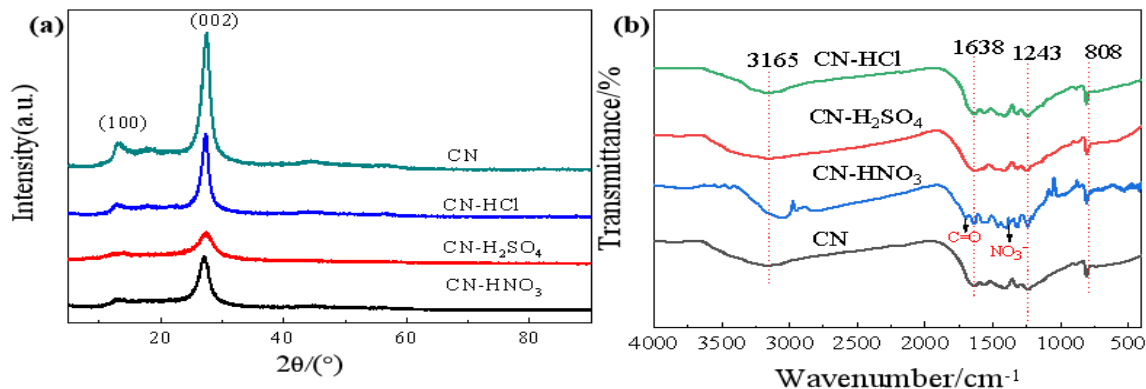


Fig. 3: (a) XRD patterns of different acid-modified carbon nitride, (b) FT-IR spectra of different catalysts.

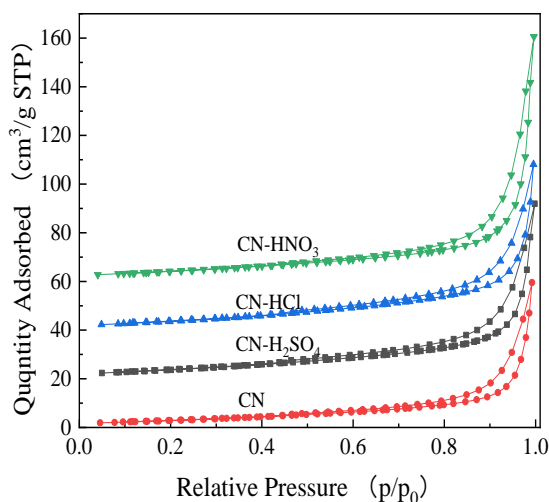


Fig. 4:  $N_2$  adsorption-desorption isotherms for preparation of catalysts.

Fig. 4 depicts the nitrogen adsorption-desorption isotherms of CN and MCN. All of the samples had type IV isotherms with an  $H_3$  hysteresis loop, indicating that a certain degree of the mesoporous structure had developed due to flake particle buildup. Mesoporous has a great influence on the activity of the reaction, which can be used as the capture site and the active site of photoexcited charge in a photochemical reaction. After calculation, the specific surface areas of CN, CN-HCl, CN-HNO<sub>3</sub>, and CN-H<sub>2</sub>SO<sub>4</sub> were 10.13, 15.16, 16.32, and 15.56  $m^2 \cdot g^{-1}$ , respectively. This result indicated that after CN modification, the catalyst had a larger specific surface area, and an increase in specific surface area, which could provide more reactive sites for the catalyst surface, and consequently lead to the improved catalytic performance of the catalyst.

Under the same relative pressure, the adsorption capacity of MCN was significantly higher than that of unmodified CN. It can also be seen that the specific surface area of MCN by nitric acid increases. In general, materials with a large specific surface area have strong adsorption capacity and a special significance in the field of nanometer and sewage purification.

XPS characterization to have a better understanding of the changes and chemical bonds of the materials, Fig. 5 (a) is the total spectrum of CN and CN-HNO<sub>3</sub>. It can be found from the graph that CN

before and after HNO<sub>3</sub> is modified contains C, N, and O elements. Fig. 5 (b) There are two characteristic peaks at 288.0 and 284.6 eV in the C1s spectrum of CN, corresponding to C-N=C and C-C bonds. showed A new generation peak can be found at 289.3 eV (C=O) in Nitric acid-modified porous CN, which may be due to the introduction of -COOH so that it has better hydrophilicity and is conducive to photocatalysis. The three characteristic peaks in the N1s spectrum in Fig. 5 (c) correspond to 398.5, 399.8, and 401.1 eV, respectively. The characteristic peak at 398.5 eV belongs to the hybridization of N atom  $sp^2$  in the C-N=C structure, while that at 399.7 and 401.1 eV corresponds to the bond energy of N-(C)<sub>3</sub>, and the bond energy of N-H. In short, the introduction of the carboxyl group makes it have better hydrophilicity, and more conducive to photocatalytic.

As shown in the SEM image in Fig. 6 (a), it can be seen that CN exhibits a very obvious stacked lamellar structure. Fig. 6 (b) is CN-HCl, which can also be seen as a smaller lamellar structure than pure CN. After modification with nitric acid and sulfuric acid, the surface of CN has many exposed pore structures in Fig. 6 (c) and (d). The reason is that the surface of CN is oxidized by acid treatment, which destroys its original structure, and a positive charge and electrostatic effect are found in MCN. These holes increase the surface area of CN, which increases the probability of reaction when contacting other substances. These pores also changed the chemical structure of CN and had a certain impact on physical and chemical properties of CN.

The degradation of RhB was used to evaluate the photocatalytic activity of CN, CN-HCl, CN-H<sub>2</sub>SO<sub>4</sub>, and CN-HNO<sub>3</sub>, and the light was turned on after 30 min. The dark reaction stage was 30 min ago. As shown in Fig. 7 (a), the catalytic efficiency of acid modification was higher than that of pure CN in the dark reaction stage. After illumination, CN, CN-HCl, CN-H<sub>2</sub>SO<sub>4</sub>, and CN-HNO<sub>3</sub> showed photocatalytic degradation efficiencies of 63.1%, 81.2%, and 85.1%, respectively. The photocatalytic activity of CN-HNO<sub>3</sub> was the greatest, with a 99.7% elimination rate of RhB after 90 minutes of light. In Fig. 7 (b), the linear relationship between  $\ln(C/C_0)$  and irradiation time can be seen from  $-\ln(C/C_0) = kt$ , indicating that the photodegradation of RhB follows the first-order reaction model. The  $k$  value represents the degradation rate, and CN, CN-HCl, CN-H<sub>2</sub>SO<sub>4</sub>, and CN-HNO<sub>3</sub> have high  $k$  values with the degradation rate constants

k of 0.0062, 0.0091, 0.0112, and 0.0341  $\text{min}^{-1}$ , respectively. CN-HNO<sub>3</sub> has good photocatalytic activity under visible light, the reason may be that the introduction of oxygen-containing functional groups increases the active sites, which is conducive to the photocatalytic process, followed by the pore structure, which is conducive to the combination with pollutants. Therefore, CN-HNO<sub>3</sub> has a good application prospect in the effective removal of RhB in the environment.

The stability of the catalyst is also one of the important indicators that affect the catalytic performance of the photocatalyst. Fig. 8 (a) showed the cyclic activity of CN-HNO<sub>3</sub> after repeats after five

cycles. After each degradation experiment, the catalyst after the reaction is obtained by centrifugal separation, washed three times with deionized water and ethanol, dried, and then subjected to the next cycle experiment. The degradation rate of RhB by the CN-HNO<sub>3</sub> barely altered marginally after five cycles, as shown in Fig. 8. At the same time, the surface of the catalyst may remain the RhB adsorbed in the previous experiment, which will also affect the degradation rate of the catalyst to a certain extent. However, the degradation rate reached above 85% after five cycles, which proved that the catalyst had good stability.

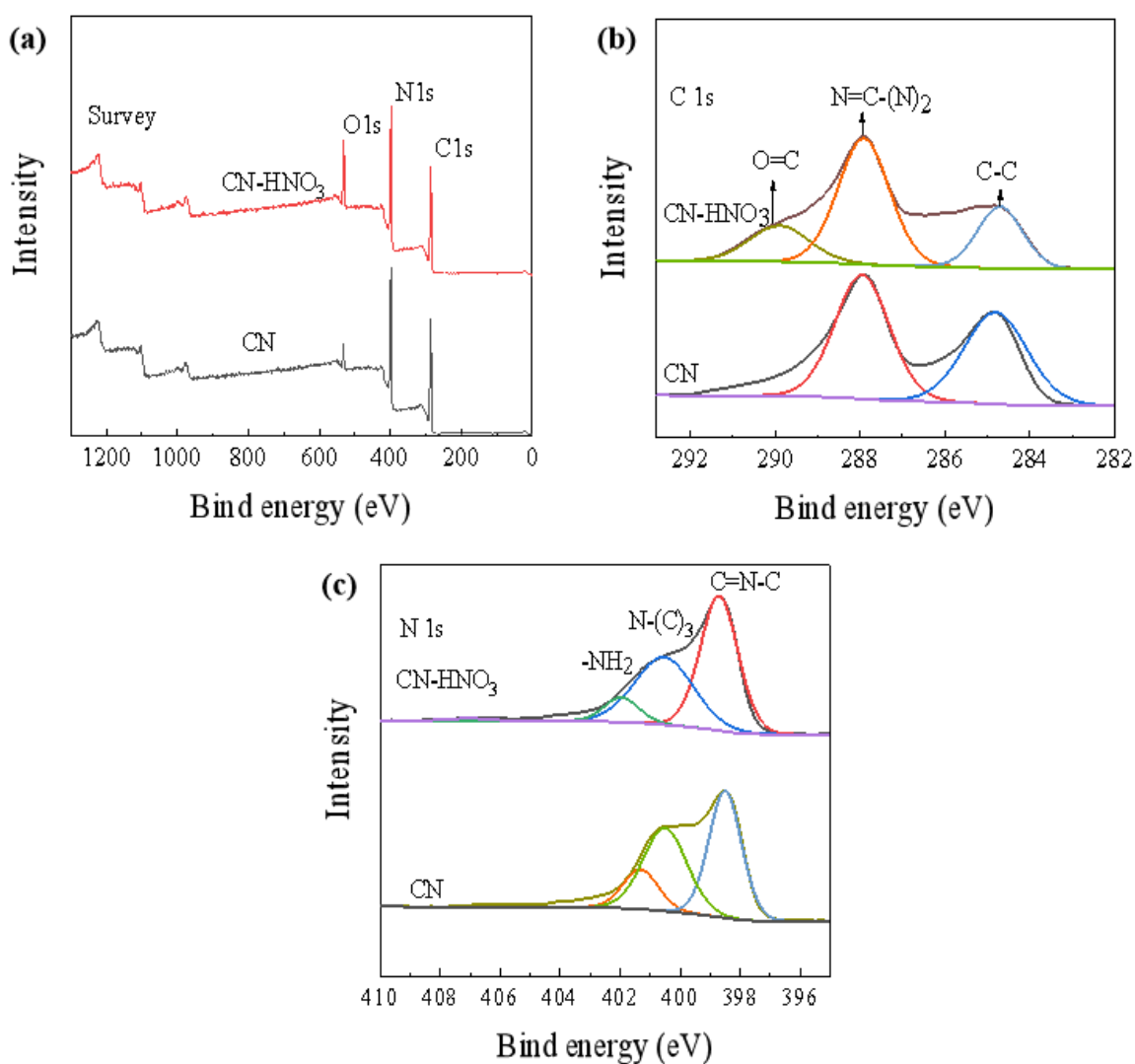


Fig. 5: XPS spectra of CN-HNO<sub>3</sub> and CN catalysts (a) Survey, (b) C1s, (c) N1s.

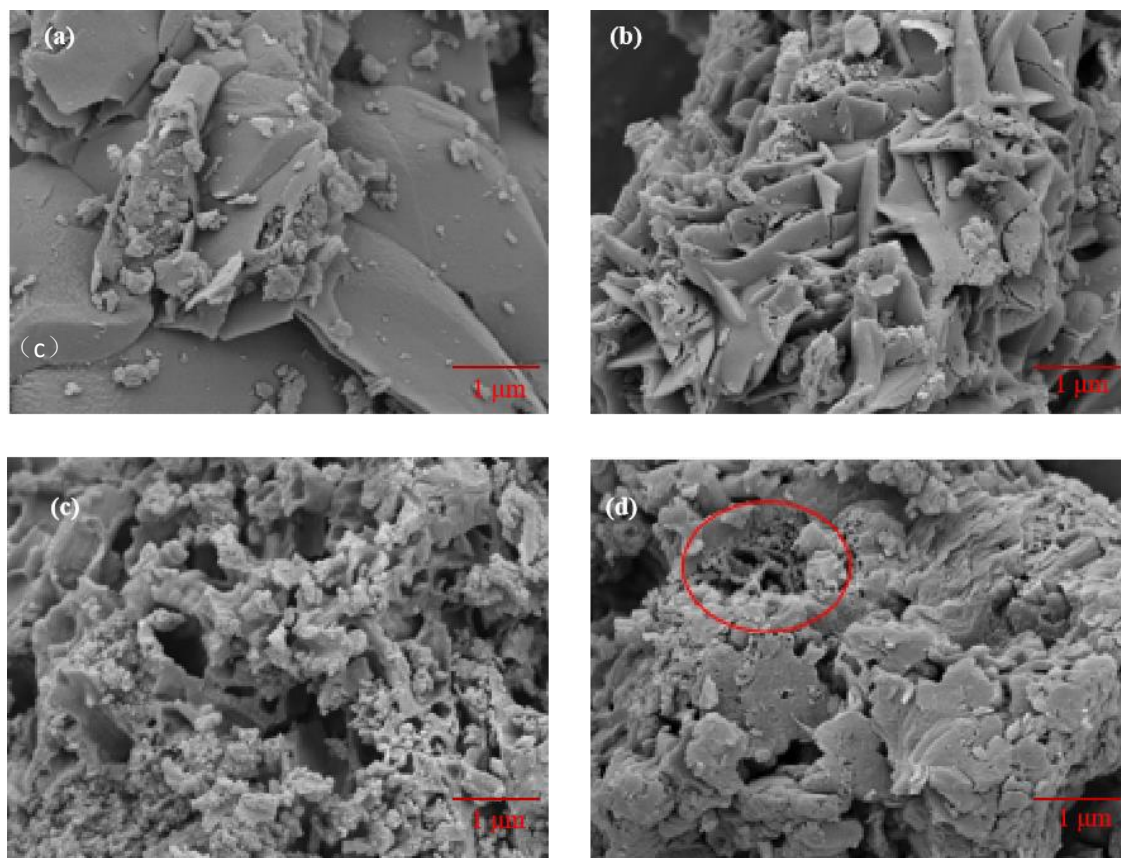


Fig. 6: SEM images of different catalysts (a) CN, (b) CN-HCl, (c) CN-H<sub>2</sub>SO<sub>4</sub> (d) CN-HNO<sub>3</sub>.

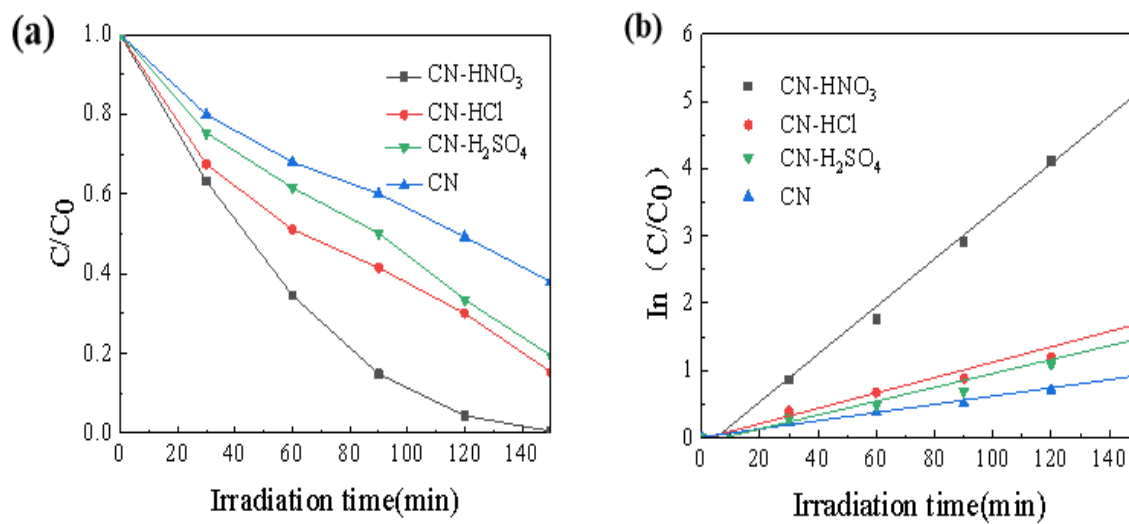


Fig. 7: (a) Degradation capacity of different catalysts for RhB, (b) Degradation rate constants of different catalysts for RhB.

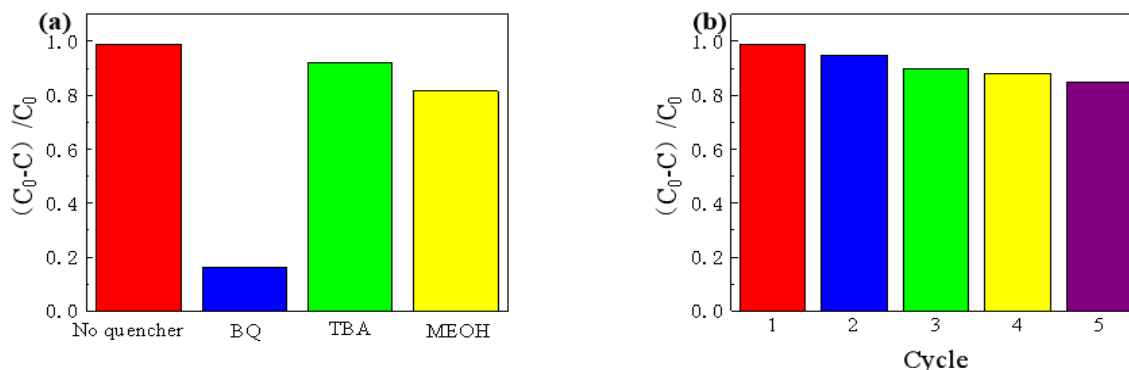


Fig. 8: (a) Cyclic activity of CN-HNO<sub>3</sub> catalyst, (b) Effect of capture agent on the photodegradation of RhB by CN-HNO<sub>3</sub>.

Free radical trapping experiments are shown in Fig. 8 (b). Under the same reaction conditions, different trapping agents were added to the reaction to determine the reactive substances. For hydroxyl radical ( $\cdot\text{OH}$ ), superoxide radical ( $\cdot\text{O}_2^-$ ), and photogenerated hole ( $h^+$ ), tert-butyl alcohol (TBA), p-benzoquinone (BQ), and methanol (MeOH) were utilized as capture agents, respectively. The photocatalytic degradation impact of RhB was investigated after the capture agent was introduced to the system to identify the effects of holes,  $\cdot\text{OH}$ , and  $\cdot\text{O}_2^-$ . Because the band value of CN-HNO<sub>3</sub> (2.49 eV) was lower than the redox potential of  $\cdot\text{OH}/\text{OH}^-$  (+1.99 eV) and  $\cdot\text{OH}/\text{H}_2\text{O}$  (+2.73 eV), the addition of TBA had minimal influence on the degradation of RhB [19,20]. When adding MEOH, the degradation rate has a certain degree of influence, indicating that  $h^+$  has a certain degree of influence and plays an auxiliary role in photocatalysis. The degradation efficiency of 16.4% with BQ was significantly lower than that without the capture agent (99.7%), indicating that superoxide radicals play a major role in the degradation of RhB. According to the findings,  $\cdot\text{O}_2^-$  had a substantial role in the degradation of RhB by CN-HNO<sub>3</sub>, with photogenerated holes playing a supporting function.

Fig. 9 (a) shows the UV-Vis DRS spectra of CN, CN-HCl, CN-HNO<sub>3</sub>, and CN-H<sub>2</sub>SO<sub>4</sub> catalysts. The absorption boundary of CN is about 459 nm, and the tangent of the absorption curve is made by the intercept method. The absorption wavelength threshold is the intersection of the tangent extension line and the X-axis. According to the optical band gap equation  $E_g = 1240/\lambda$  [21], the bandgap energy of CN is 2.70 eV. The absorption band edges of CN, CN-HCl, CN-HNO<sub>3</sub>, and CN-H<sub>2</sub>SO<sub>4</sub> catalysts were about 450, 464, and 497 nm, respectively, which were red-shifted compared with CN. The corresponding band gap

energies were 2.76 and 2.49 eV, respectively, indicating that the modification of different acids could adjust the bandgap width of the catalyst. Among them, the bandgap width of the catalyst modified by nitric acid was the lowest, and the decrease in the bandgap energy increased the absorption of light by the catalyst, resulting in more electron-hole pairs.

Because the bandgap of CN-HNO<sub>3</sub> is narrower than that of pure CN, it can trigger more photogenerated electrons and holes when exposed to visible light. The optical absorption threshold of CN is around 459 nm, and its bandgap is estimated to be 2.70 eV, according to the DRS study. The valence band (VB) of the XPS valence band spectrum is shown in Fig. 9 (b). The value of CN is 1.57 eV. As a result, using the empirical formula: The conduction band location of CN is determined to be 1.13 eV using  $E_{\text{CB}} = E_{\text{VB}} - E_g$ .  $\cdot\text{OH}/\text{OH}^-$  and  $\text{O}_2/\cdot\text{O}_2^-$  have redox potentials of +1.99 and -0.33 eV [22], respectively. As a result, while the electrons on pure CN (1.13 eV) CB can decrease  $\text{O}_2$  to  $\cdot\text{O}_2^-$ , the VB position is insufficient to oxidize  $\cdot\text{OH}$  to  $\text{OH}^-$ . The bandgap of CN-HNO<sub>3</sub> material is calculated to be 2.49 eV, while the optical absorption threshold is around 497 nm.

The separation of photogenerated electron-hole pairs by photoluminescence spectroscopy is studied in PL characterization [23], and the findings are displayed in Fig. 9 (c). Compared with CN, the luminescence rate of CN-HNO<sub>3</sub> material at 450 nm decreased significantly. It is known that the emission peak of PL comes from the quenching of photogenerated electron-hole pairs, that is, the higher the recombination rate of photogenerated electron-hole pairs, the stronger the PL peak intensity. It can be seen that the modification of acid significantly improves the separation efficiency of the electron hole

in the catalyst. On the one hand, maybe the modification of acid makes the specific surface area increase and thus increase a lot of active sites, on the other hand, the introduction of the carboxyl group can quickly transfer the photo charge, inhibit the recombination of photogenerated electron-hole pairs inhibit the recombination of photogenerated electron-hole pairs so that the catalyst has higher photocatalytic activity.

Fig. 9 (d) Photocatalytic mechanism shows that CN-HNO<sub>3</sub> plays electrostatic adsorption on the surface of CN-HNO<sub>3</sub> due to the formation of -COOH, and the VB of CN-HNO<sub>3</sub> is -1.23 eV, and the VB of CN is -1.13 eV. Compared with CN, CN-HNO<sub>3</sub> is easier to reduce O<sub>2</sub> to ·O<sub>2</sub><sup>-</sup>, and produce more ·O<sub>2</sub><sup>-</sup>. CN-HNO<sub>3</sub> plays electrostatic adsorption on RhB due to the formation of -COOH, and adsorbs on the surface of CN-HNO<sub>3</sub>, making ·O<sub>2</sub><sup>-</sup> easier to degrade RhB. The photocatalytic efficiency was improved.

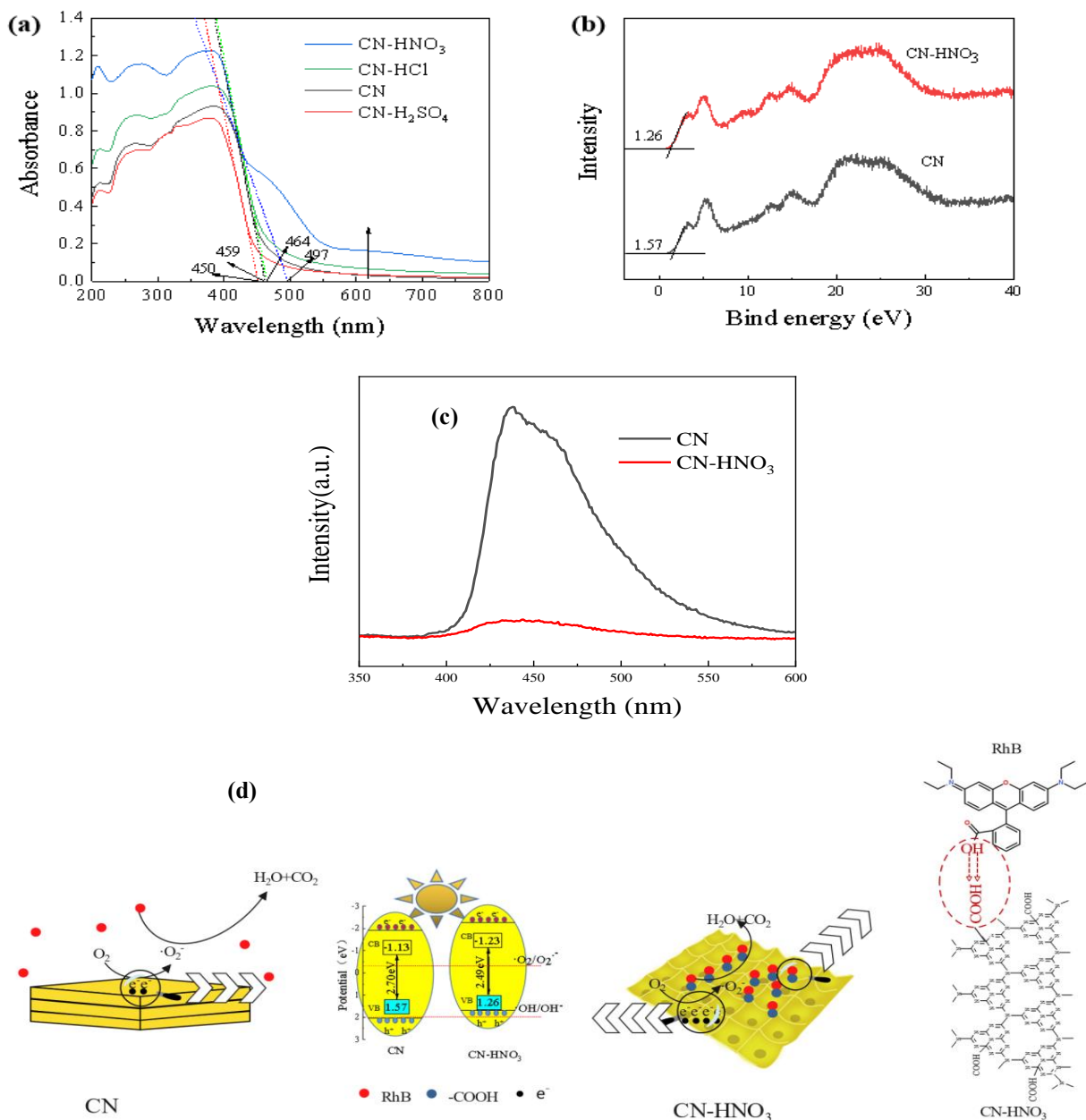


Fig. 9: (a) UV-Vis DRS spectra of different catalysts, (b) XPS valence bands of CN and CN-HNO<sub>3</sub>, (c) PL spectra of CN and CN-HNO<sub>3</sub> catalysts, (d) Photocatalytic mechanism diagram of CN and CN-HNO<sub>3</sub>

## Conclusion

This study proposed a simple and efficient method to prepare CN and MCN with block- and pore morphologies. The results indicate that the MCN particles are all anhydrous magnesium carbonate crystals, which can significantly improve the photocatalytic efficiencies of CN, especially the degradation rate constant. Moreover, CN-HNO<sub>3</sub> has a uniform cube-like shape, a small size, active sites, bandgap width, and outstanding photocatalytic efficiencies of 99.7%. The degradation rate constant of CN-HNO<sub>3</sub> for RhB is 0.0341 min<sup>-1</sup>, which is 5.5 times of unmodified CN. After five cycles, the degradation efficiency is still higher than 85%, indicating the decrease of bandgap energy increased the absorption of light by the catalyst and generated more electron-hole pairs, and the VB of CN-HNO<sub>3</sub> was smaller than that of CN. CN-HNO<sub>3</sub> is easier to reduce O<sub>2</sub> to ·O<sub>2</sub><sup>-</sup>, which is more conducive to photocatalytic performance. The free radical trapping experiments showed that the photocatalytic activity of CN-HNO<sub>3</sub> was enhanced by the synergistic effect of ·O<sub>2</sub><sup>-</sup> and hole. Carbon nitride modified by a sample preparation method has high catalytic efficiency and is easier to industrialize. This study confirms that CN-HNO<sub>3</sub> material has broad application potential in the degradation of organic pollutants and is expected to develop in a clean environment for a long time.

## Acknowledgments

This project was supported by the special project of the Qinghai Provincial Department of science and technology (2021-SF-132), the innovation project of Kunlun elitist of Qinghai Province, and training program for famous teachers of Qinghai University (SYJG2020008).

## Conflict of Interest

The authors declare no conflict of interest.

## References

1. D. Esposito, M. Antonietti, Redefining biorefinery: the search for unconventional building blocks for materials. *Chem Soc Rev*, **44**, 5821 (2015).
2. F. H. Isikgor, C. R. Becker, Lignocellulosic biomass: a sustainable platform for the production of bio-based chemicals and polymers. *Polym. Chem.* **6**, 4497 (2015).
3. I. F. Teixeira, E. Barbosa, S. Tsang, P. Camargo, Carbon nitrides and metal nanoparticles: From controlled synthesis to design principles for improved photocatalysis. *Chem Soc Rev.* **47** (2018).
4. Y. Zhu, C. Romain, C. K. Williams, Sustainable Polymers from Renewable Resources. *Nature*, **540**, 354 (2016).
5. L. Wang, G. Zhou, Y. Tian, L. Yan, M. Deng, B. Yang, Z. Kang, H. Sun, Hydroxyl Decorated g-C<sub>3</sub>N<sub>4</sub> Nanoparticles with Narrowed Bandgap for High Efficient Photocatalyst Design. *Appl. Catal. b*, **244**, 262 (2019).
6. M. Sumathi, A. Prakasam, P. M. Anbarasan., Fabrication of Hexagonal Disc Shaped Nanoparticles g-C<sub>3</sub>N<sub>4</sub>/NiO Heterostructured Nanocomposites for Efficient Visible Light Photocatalytic Performance. *J. Cluster sci.* **30**, 757 (2019).
7. Q. Cao, B. Kumru, M. Antonietti, B. V. K. J. Schmidt, Graphitic Carbon Nitride and Polymers: A Mutual Combination for Advanced Properties. *Mater. Horiz.* **7**, 762 (2019).
8. D. Huang, X. Yan, Y. Ming, G. Zeng, C. Zhou, J. Wan, M. Cheng, W. Xue, Graphitic Carbon Nitride-Based Heterojunction Photoactive Nanocomposites Applications and Mechanism Insight. *Acs Appl Mater Inter.* **10**, 8b03620- (2018).
9. H. Yu, L. Shang, T. Bian, R. Shi, T. Zhang, Carbon Nanosheets: Nitrogen-Doped Porous Carbon Nanosheets Templated from g-C<sub>3</sub>N<sub>4</sub> as Metal-Free Electrocatalysts for Efficient Oxygen Reduction Reaction, *Adv Mater*, **28**, 5140 (2016).
10. Y. Hong, E. Liu, J. Shi, X. Lin, L. Sheng, M. Zhang, L. Wang, J. Chen, A Direct One-Step Synthesis of Ultrathin g-C<sub>3</sub>N<sub>4</sub> Nanosheets from Thiourea for Boosting Solar Photocatalytic H<sub>2</sub> Evolution. *Int. J. Hydrogen energy*, **44**, 7194 (2019).
11. B. Coulson, L. Lari, M. Isaacs, D. J. Raines, R. E. Douthwaite, A. Duhme-Klair, Carbon Nitride as a Ligand: Selective Hydrogenation of Terminal Alkenes Using [(η<sup>5</sup>-C<sub>5</sub>Me<sub>5</sub>) IrCl (g-C<sub>3</sub>N<sub>4</sub>-κ<sup>2</sup>N, N')] Cl. *Chem. - Eur. J.* **26**, 6862 (2020).
12. Y. Ren, D. Zeng, W. J. Ong, Interfacial Engineering of Graphitic Carbon Nitride (g-C<sub>3</sub>N<sub>4</sub>)-Based Metal Sulfide Heterojunction Photocatalysts for Energy Conversion: A Review. *Chin. J. Catal.* **40**, 289 (2019).
13. H. Yu, L. Shang, T. Bian, R. Shi, G. Waterhouse, Y. Zhao, C. Zhou, L. Z. Wu, C. Tung, T. Zhang, Carbon Nanosheets: Nitrogen-Doped Porous Carbon Nanosheets Templated from g-C<sub>3</sub>N<sub>4</sub> as Metal-Free Electrocatalysts for Efficient Oxygen

- Reduction Reaction, *Adv Mater.* **28** (2016).
14. M. Wu, J. Zhang, B. He, H. Wang, R. Wang, Y. S. Gong, In-situ construction of coral-like porous P-doped g-C<sub>3</sub>N<sub>4</sub> tubes with hybrid 1D/2D architecture and high efficient photocatalytic hydrogen evolution. *Appl Catal B-Environ*, **241**, 159 (2019).
  15. Y. Xu, F. Ge, Z. Chen, S. Huang, W. Wei, M. Xie, H. Xu and H. Li, One-step synthesis of Fe-doped surface-alkalinized g-C<sub>3</sub>N<sub>4</sub> and their improved visible-light photocatalytic performance. *Appl Surf Sci.* **469**, 739 (2019).
  16. S. Cao, Q. Huang, B. Zhu, J. Yu, Trace-level phosphorus and sodium co-doping of g-C<sub>3</sub>N<sub>4</sub> for enhanced photocatalytic H<sub>2</sub> production. *J. Power sources*, **351**, 151 (2017).
  17. H. J. Li, B. W. Sun, L. Sui, D. J. Qian, M. Chen, Preparation of water-dispersible porous g-C<sub>3</sub>N<sub>4</sub> with improved photocatalytic activity by chemical oxidation. *Phys. Chem. Chem. Phys.* **17**, 3309 (2015).
  18. H. Wei, Q. Zhang, Y. Zhang, Z. Yang, A. Zhu, D. D. Dionysiou, Enhancement of the Cr(VI) adsorption and photocatalytic reduction activity of g-C<sub>3</sub>N<sub>4</sub> by hydrothermal treatment in HNO<sub>3</sub> aqueous solution. *Appl Catal A-Gen.* **521**, 9 (2016).
  19. S. Cao, J. Low, J. Yu, M. Jaroniec, Polymeric Photocatalysts Based on Graphitic Carbon Nitride. *Adv Mater.*, **27** (2015).
  20. F. Chang, J. Zhang, Y. Xie, J. Chen, C. Li, J. Wang, J. Luo, B. Deng, X. Hu, Fabrication, characterization, and photocatalytic performance of exfoliated g-C<sub>3</sub>N<sub>4</sub>-TiO<sub>2</sub> hybrids. *Appl Surf Sci.* **311**, 574 (2014).
  21. A. Kudo, Y. Misaki, Heterogeneous photocatalyst materials for water splitting. *Chem Soc Rev.* **38**, 253 (2008).
  22. Y. Zheng, J. Liu, J. Liang, M. Jaroniec, S. Z. Qiao, Graphitic carbon nitride materials: controllable synthesis and applications in fuel cells and photocatalysis. *Energy Environ. Sci.* **5**, 6717 (2012).
  23. X. Li, Z. Jian, L. Shen, Y. Ma, W. Lei, O. Cui, G. Zou, Preparation and characterization of graphitic carbon nitride through pyrolysis of melamine. *Appl Catal A-Gen.* **94**, 387 (2009).